Computers in Biology and Medicine 115 (2019) 103482

Contents lists available at ScienceDirect

Computers in Biology and Medicine

journal homepage: http://www.elsevier.com/locate/compbiomed

Novel application of the gray-level co-occurrence matrix analysis in the parvalbumin stained hippocampal gyrus dentatus in distinct rat models of Parkinson's disease

Nemanja Rajkovic [b,*], Jelena Ciric [a], Nebojsa Milosevic [b], Jasna Saponjic [a]

[a] University of Belgrade, Department of Neurobiology, Institute for Biological Research - Sinisa Stankovic, Belgrade, Serbia
[b] University of Belgrade, School of Medicine, Department of Biophysics, Belgrade, Serbia

ARTICLE INFO

Keywords:
Image analysis
Gray-level co-occurrence matrix analysis
Fractal analysis
Hippocampal gyrus dentatus
Parvalbumin
GABA interneurons
Cholinopathy of Parkinsons' disease
Hemiparkinsonism
Rat

ABSTRACT

To reveal the best choice of algorithm for parvalbumin-immunostained images of the hippocampal gyrus dentatus in two distinct rat models of Parkinson's disease (PD), particularly in terms of extracting the crucial information from the image, we tested whether the impact of experimentally induced dopaminergic (hemiparkinsonism) vs. cholinergic (PD cholinopathy) innervation impairment on the parvalbumin stained GABA interneurons could be detected using two separate algorithms, the fractal box-count and the gray-level co-occurrence matrix analysis (GLCM) algorithms.

For the texture and fractal analysis of the hippocampal gyrus dentatus images, we used.tif images from three experimental groups of adult male Wistar rats: control rats, rats with Parkinson disease (PD) cholinergic neuropathology (with a PPT lesion), and hemiparkinsonian rats (with a SNpc lesion).

For the suprapyramidal layer of the gyrus dentatus *ASM* and *Entropy* differentiated the images of the SNpc lesion versus the images of the control and the PPT lesion subjects, with significantly higher *ASM* and lower *Entropy*, indicating the homogenization of the images and their lower gray-level complexity. The infrapyramidal images of the SNpc group were differentiated versus the images from the control and PPT groups in terms of all the GLCM parameters: they showed lower mean *Entropy* and *Contrast* and higher *ASM*, *Correlation* and *IDM*.

These results strongly suggest a rise in the uniformity, homogeneity and orderliness in the gray-levels of images from the SNpc group.

Our results indicate that GLCM analysis is a more sensitive tool than fractal analysis for the detection of increased dendritic arborization in histological images.

1. Introduction

In the past two decades, clinical and scientific interest in computational image analysis has risen, due to increases in computational power and comfort in extracting the relevant information from grayscale images [1].

The main advantage of the computational analysis of brain tissue images stems from its ability to investigate all the visible structures without discrimination and deal with spatial changes in pixel intensities not distinguishable to the human eye. Moreover, computer-aided image analysis has emerged as a tool which might complement the established approaches as it measures features that previously could not be identified quantitatively, or could not be identified at all [2–4]. Fractal and gray-level co-occurrence matrix (GLCM), along with machine learning algorithms, are among the most commonly used image analysis algorithms.

Many natural objects exhibit complexity and irregularity that is hard, if not impossible, to adequately describe using regular Euclidean geometry. As a consequence, fractal geometry has arisen, which has been called "the geometry of nature". It has developed for more than a century with the aim of overcoming the shortcomings of regular geometry in quantitatively describing irregular natural systems. The original idea of Hausdorff and Besicovitch of a fractional dimension was further developed and popularized by Benoit Mandelbrot [5], who also coined the term "fractal", thus starting a prolific period of fractal analysis. The non-linear character of such analysis renders it quite useful for naturally

* Corresponding author. Department of Biophysics, School of Medicine, University of Belgrade, Visegradska 26/2, 11000, Belgrade, Serbia.
E-mail address: nemanja.rajkovic@med.bg.ac.rs (N. Rajkovic).

https://doi.org/10.1016/j.compbiomed.2019.103482
Received 18 July 2019; Received in revised form 16 September 2019; Accepted 3 October 2019
Available online 4 October 2019
0010-4825/

occurring objects and signals. Fractal geometry has found its way into a wide range of natural morphology analyses, including images of the brain [4,6,7], even allowing for the methodological limitation which arises from the fact that natural objects are not ideal fractals, but rather exhibit fractal properties of self-similarity and infinite complexity on a limited range of scales. Initially, fractal analysis was performed on binary images with only black and white pixels, and this still remains one of the most commonly used methods. However additional methods, such as differential box-counting, have been developed to make a grayscale fractal analysis possible [8].

In addition, GLCM analysis is another commonly used type of image analysis. It is a statistical method based on second-order statistics and regarded as the most popular type of texture analysis [9,10]. First introduced in 1973 by Haralick et al. [11], GLCM is used on 256-bit grayscale images which are information-rich, and therefore superior to the binary fractal analysis for texture based images, such as histological images [12]. This method quantifies the distribution of gray level intensities within a group of pixels thus extracting information about tone homogeneity, their linear connection, contrast within the image and the boundaries between the gray tones and the complexity of their distribution [11].

Our focus in this study was to test the applicability and sensitivity of the fractal box-count and GLCM algorithms on the parvalbumin-immunostained images of the hippocampal gyrus dentatus in two distinct rat models of Parkinson's disease. Particularly, we tested whether the impact of the experimentally induced dopaminergic (hemiparkinsonian rats) vs. cholinergic (Parkinson disease cholinopathy) innervation impairment on the parvalbumin stained GABA interneurons of the hippocampal gyrus dentatus could be detected using two separate algorithms, to reveal the algorithm that represented the best choice for this type of image, in terms of extracting the crucial information from the image, either from its morphological characteristics or from its texture.

2. Material and methods

2.1. Experimental design

For the texture and fractal analysis of the hippocampal gyrus dentatus images, we used.tif images, all of which had a size of 2088 × 1550 pixels and a resolution of 300 dpi, from three experimental groups of adult male Wistar rats: control rats (n = 5), rats with Parkinson disease (PD) cholinergic neuropathology (via a PPT lesion; n = 4), and hemiparkinsonian rats (with an SNpc lesion; n = 4). Overall there were 47 images (of which 26 were suprapyramidal and 21 infrapyramidal) from 5 control rats, 35 images (of which 20 were suprapyramidal and 15 infrapyramidal) from 4 rats with PD cholinopathy (with a PPT lesion), and 41 images (being 22 suprapyramidal and 19 infrapyramidal images) from 4 hemiparkinsonian rats (with an SNpc lesion).

The surgical procedure, staining and image preparation was done at the Institute for Biological Research – Sinisa Stankovic of the University of Belgrade. The image analysis was done at the Institute of Biophysics, part of the School of Medicine at the University of Belgrade.

2.2. Surgical procedure

Prior to surgery and throughout the experimental protocol, the animals were maintained on a 12 h light-dark cycle (7 a.m. lights on, 7 p.m. lights off) and were housed at 25 °C with free access of food and water. This study was carried out in accordance with the recommendations of EEC Directive (2010/63/EU) on the Protection of Animals used for Experimental and Other Scientific Purposes, and the protocol was approved by the Ethical Committee for the Use of Laboratory Animals of the Institute for Biological Research "Sinisa Stankovic" at the University of Belgrade (Approval N^{O} 2–21/10).

The PD cholinopathy of Wistar rats was induced by a bilateral excitotoxic lesion of the pedunculopontine tegmental nucleus (PPT) using a stereotaxically guided microinfusion of 0.1 M of an ibotenic acid (IBO; Sigma-Aldrich, St. Louis, MO, USA; pH = 7.4) solution in 0.1 M of phosphate buffered saline (PBS), directly into the PPT (A/P: -7.8 mm from the bregma; R/L: 1.9 mm from the sagittal suture; D/V: 7.0 mm from the brain surface, following Paxinos and Watson [13]). The hemiparkinsonism of Wistar rats was induced by a unilateral lesion of the substantia nigra pars compacta (SNpc) by using 2 µl of 6 µg/µl of 6-hydroxy dopamine hydrobromide salt (6-OHDA; Sigma-Aldrich, St. Louis, MO, USA) dissolved in ice-cold sterile saline (0.9% NaCl) and supplemented with 0.2% ascorbic acid (as an antioxidant), directly into the right SNpc (A/P: -5.3 mm from the bregma; R: 2.4 mm from the sagittal suture; D/V: 7.4 mm from the brain surface, following Paxinos and Watson [13]). In addition, to minimize the uptake of 6-OHDA by noradrenergic neurons, 30 min prior to the microinfusion, each rat received a bolus of desipramine hydrochloride (28.42 mg/kg, i.p., Sigma-Aldrich, St. Louis, MO, USA; pH = 7.4).

For all the microinfusions we used a Digital Lab Standard Stereotaxic Instrument (Stoelting Co., Europe) with a Hamilton syringe (10 µl). While the microinfusions of IBO into the PPT were introduced at a volume of 100 nl, using a single 60 s pulse, the microinfusions of 6-OHDA into the right SNpc were done as a single pulse of 200 nl/min at a constant flow rate, over 10 min [14,15]. Following each microinfusion the Hamilton syringe was left within the local brain tissue for 5 min before its removal from the brain, allowing the solution to diffuse within the PPT or SNpc.

2.3. Tissue processing and quantification of the parvalbumin immunostained cells (the parvalbumin-expressing interneurons)

All the rats were deeply anesthetized and perfused transcardially, starting with a vascular rinse until the liver had been cleared (200 ml of 0.9% saline at a perfusion speed of 40 ml/min); followed by a 4% paraformaldehyde solution in 0.1 M PBS (200 ml; initially 100 ml at 40 ml/min, and then 30 ml/min), and finally with a 10% sucrose solution in 0.1 M PBS (200 ml at 30 ml/min). The animals were sacrificed and the brains were extracted, cleared of the meninges and blood vessels, and immersed in 4% paraformaldehyde overnight, and then in a 30% sucrose solution for several days. The brains were cut in the coronal plane into 40 µm-thick sections using a cryotome (Leica, Wetzlar, Germany), and the free-floating sections were further stored in a cryoprotective buffer (0.05 M phosphate buffer, 25% glycerol, and 25% ethylene glycol) at −20 °C [14–16].

Parvalbumin immunohistochemistry was performed under the same conditions for all the experimental samples. The brain sections were initially thoroughly rinsed with 0.1 M PBS at pH = 7.4. The endogenous peroxidase activity was neutralized using 3% hydrogen peroxide/10% methanol in 0.1 PBS for 15 min, and the nonspecific binding was prevented by 60 min of incubation in 5% normal donkey serum (D9663, Sigma-Aldrich, USA)/0.1 M PBS at RT [14]. The sections were further incubated for 24 h at 4 °C with a primary mouse monoclonal anti-PV antibody (dil. 1:2000, P3088, Sigma-Aldrich, USA) in a blocking solution with 0.5% Triton X-100, and subsequently for 90 min in polyclonal rabbit anti-mouse immunoglobulin (dil. 1:100, Agilent Dako, P0260, Denmark). Between each immunolabeling step, the sections were washed in fresh 0.1 M PBS (3 × 5 min). The immunoreactive signals were visualized using a diaminobenzidine solution (1% 3,3′-diaminobenzidine [11208, Acros organics]/0.3% hydrogen peroxide/0.1 M PBS). All the sections were finally mounted on slides, dehydrated in a series of increasing ethanol solutions (Ethanol of 70%, 96%, 100%, Zorka Pharma, RS), placed in a clearing agent (Xylene, Zorka Pharma, RS), mounted with DPX (Sigma-Aldrich, USA), coverslipped and examined under a Zeiss Axiovert microscope with a camera. To test immunolabeling specificity, the primary antibodies were omitted in the control experiments.

The immunohistochemistry was performed under the same

conditions for all the experimental samples, and the parvalbumin immunostained cells of the gyrus dentatus was quantified by using the Image J 1.49v software.

All the images we used were from the hippocampal gyrus dentatus of the same caudality (Fig. 1; −3.0 mm caudal to bregma, following Paxinos and Watson [17]).

For the parvalbumin-expressing interneurons quantification, the texture and fractal analysis we used at least three suprapyramidal and two infrapyramidal images of the hippocampal gyrus dentatus granular layer for each rat in each experimental group, and for each brain side (Fig. 2).

2.4. Image analysis

Prior to analysis of all the images, in order to reduce the effect of the different amount of coloring of individual samples, we performed Color Match by using the Adobe Photoshop CC (Version 14.0) toolbox and the same software was used to transform the images into grayscale (Fig. 2).

2.5. Gray-level co-occurrence matrix (GLCM) analysis

All the parameters of the GLCM analysis were calculated using the *Texture Analyzer* plugin for the java based ImageJ 1.49v software [18]. GLCM quantifies the spatial probability distributions of the gray-level values between the pairs of pixels in an image [11]. The distance and angle of orientation between the pixels in a pair may vary (0°, 45°, 90° and 135°). In this study, the distance was set to 1 and the orientation was fixed at an angle of 0°. The gray-level intensities varied from 0 to 255. We calculated five statistical GLCM features: contrast, correlation, entropy, inverse difference moment (IDM) and angular second moment (ASM). Contrast carries information about the relative difference in gray-level values between the adjacent pixels. Correlation measures the linear dependency of the gray levels on those of neighboring pixels, which means that if there is a high value of correlation, there is a predictable and linear relationship between the neighboring pixels given by the regression equation. Entropy carries information about the amount of information combined with the complexity of the image, while IDM represents the local homogeneity of the image and ASM represents its texture uniformity [19]. The software plugin calculations were performed based on the formulas provided in the original work of Haralick [11] and in the work by Hall-Beyer [19].

The GLCM consists of terms (probabilities) that state the relationship between pairs of pixels. If $P_{i,j}$ is the probability that a referent pixel and a neighboring pixel will have particular values, where i and j define the term's position in the GLCM, then the angular second moment is defined as

$$ASM = \sum_{i}\sum_{j} P_{i,j}^{2}. \tag{1}$$

contrast is defined as

$$Contrast = \sum_{i,j=0}^{N-1} P_{i,j}(i-j)^{2}. \tag{2}$$

and correlation as

$$Correlation = \sum_{i,j=0}^{N-1} P_{i,j}\left[\frac{(i-\mu_i)(j-\mu_j)}{\sqrt{(\sigma_i^2)(\sigma_j^2)}}\right], \tag{3}$$

where μ_i and μ_j are the GLCM means based on the probability of the occurrence of particular reference and neighboring pixel values given as $\mu_i = \sum_{i,j=0}^{N-1} i(P_{i,j})$ and $\mu_j = \sum_{i,j=0}^{N-1} j(P_{i,j})$, respectively, and σ_i and σ_j are GLCM standard deviations given as the square roots of the respective GLCM variances $\sigma_i^2 = \sum_{i,j=0}^{N-1} (P_{i,j})(i-\mu_i)^2$ and $\sigma_j^2 = \sum_{i,j=0}^{N-1} (P_{i,j})(j-\mu_j)^2$. The inverse difference moment is defined as

$$IDM = \sum_{i,j=0}^{N-1} \frac{P_{i,j}}{1+(i-j)^2}, \tag{4}$$

and entropy is defined as

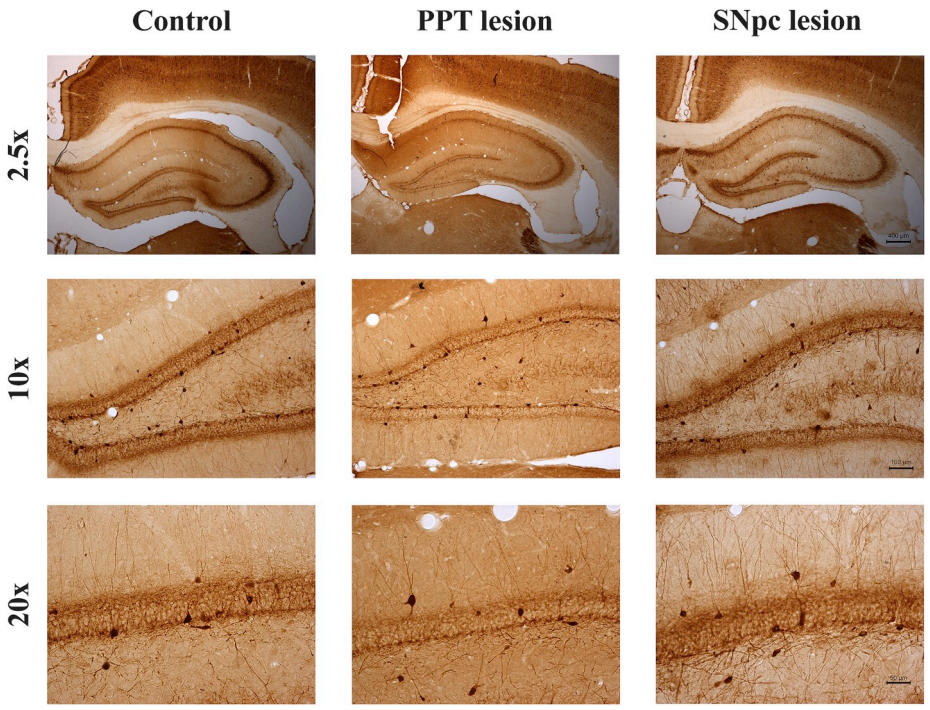

Fig. 1. Individual examples of the typical hippocampal sections and their gyri dentati used for the texture and fractal analysis. The texture and fractal analysis were done using the 20× magnified images (scale bar 50 μm) of the suprapyramidal and infrapyramidal layer of the hippocampal gyrus dentatus.

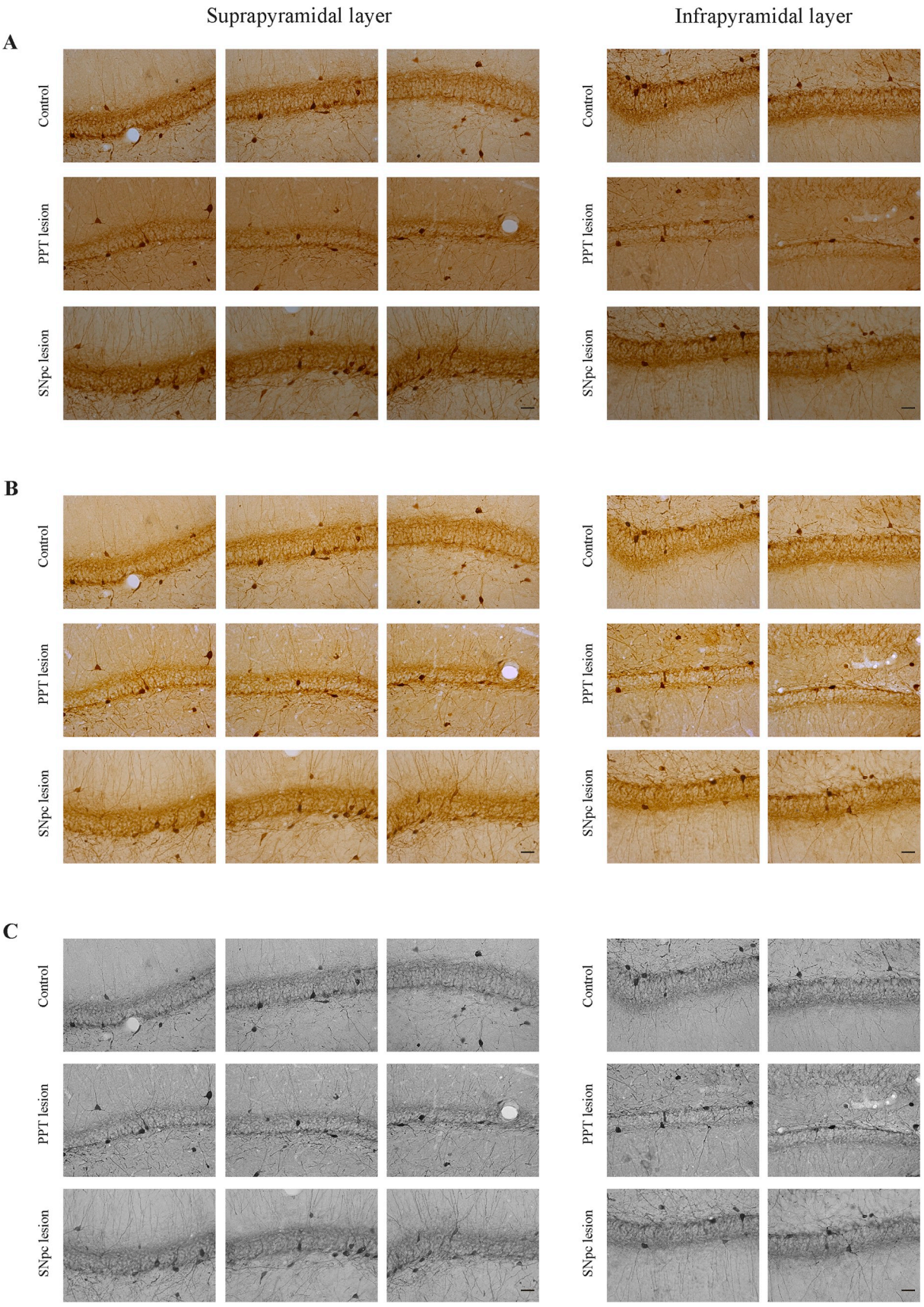

Fig. 2. Individual examples of the original (**A**), color matched (**B**), and the gray-scale (**C**) images from each experimental group (Control, PPT lesion and SNpc lesion), of the suprapyramidal and infrapyramidal part of the hippocampal gyrus dentatus used for image analysis. The scale bar for all the images is 50 μm.

$$Entropy = \sum_{i,j=0}^{N-1} P_{i,j}\left(-\ln P_{i,j}\right). \quad (5)$$

2.6. Fractal analysis

2.6.1. Binary images

Fractal analysis was performed using the ImageJ plugin FracLac version 2015marb6206 applying the regular non-overlapping box count method [20]. All the images were binarized using the default threshold value defined by the software. The background was locked to white in order to avoid any erroneous background-foreground inversion during the calculations. Outlining was performed on the binary images using the "outline" command in the software.

Two main features were calculated using the box-counting algorithm: fractal dimension and lacunarity, which are measures of complexity and heterogeneity, respectively. The box-counting method consists of covering the image with a grid of boxes of varying sizes ε and counting the minimum number of boxes (N) that contain foreground pixels of the image [21]. Fractal dimension is derived from the relationship between the number of boxes that contain the object in an image (N) and the size of those boxes (ε). It is defined as the negative limit of the ratio of the logarithms of the number of boxes and their size [20].

$$D = -\lim_{\varepsilon \to 0} \frac{\log N(\varepsilon)}{\log(\varepsilon)}. \quad (6)$$

Given that naturally occurring fractals represented by digital images do not exhibit fractal properties on the infinite scale assumed by this limit, the fractal dimension is estimated as the negative slope of the straight part of the regression line, called the fractal window [22].

Lacunarity is a measure of the heterogeneity and rotational invariance of an image. Patterns that have larger, numerous and unevenly sized gaps generally have higher values of lacunarity, while patterns with similarly sized gaps with little rotational variance have lower values. The calculation of lacunarity relies on pixel mass distribution, where the number of pixels for all box sizes (ε) is estimated, again using the box-counting method. Lacunarity at the particular size of the box ε was calculated as the square of the coefficient of variation

$$\lambda_\varepsilon = \left(\frac{\sigma}{\mu}\right)^2, \quad (7)$$

where σ stands for the standard deviation and μ for the mean of the foreground pixels per each box of the size ε.

From these lacunarity values, a single number was calculated as mean lacunarity Λ for the total number of box sizes (E) as

$$\Lambda = \frac{\sum \lambda_\varepsilon}{E}. \quad (8)$$

The minimum size of the box was set to 1 pixel and the maximum was set to 45% of the total image. This maximum size was chosen to avoid all boxes larger than the one containing all the pixels from impacting the slope, as they would have the same count value of 1. The binary parameters included binary and outline fractal dimensions (D_{bin}, D_{out}) and binary lacunarity (Λ_{bin}).

2.6.2. Grayscale images

Fractal analysis on the grayscale images was performed using the differential box-counting method in the FracLac plugin mentioned above. The calculated features for this type of image were the fractal dimension and lacunarity and were marked as D_{gray} and Λ_{gray}. While the previously mentioned box-counting identifies the number of boxes containing foreground pixels, differential box-counting calculates the difference in intensity of the pixels in the box. For a box at the size ε, the difference $\delta I_{i,j,\varepsilon}$ is calculated as

$$\delta I_{i,j,\varepsilon} = \text{maximum pixel intensity } (i,j,\varepsilon) - \text{minimum pixel intensity } (i,j,\varepsilon). \quad (9)$$

This range is increased by one in order to prevent zero values in the subsequent logarithm calculations. The sum of all differences I_ε is given as

$$I_\varepsilon = \sum \left(1 + \delta I_{i,j,\varepsilon}\right). \quad (10)$$

The grayscale box-count dimension Dgray is calculated [20] from the regression line of the logarithmic graph of the I_ε and the box sizes (ε)

$$D_{gray} = \lim_{\varepsilon \to 0} \frac{\log(I_\varepsilon)}{\log\left(\frac{1}{\varepsilon}\right)}. \quad (11)$$

2.7. Statistical analysis

All the statistical analysis were performed using a Kruskal-Wallis ANOVA (X^2-values) and a Mann-Whitney U (z - values) two-tailed *post hoc* test. The accepted level of significance was $p \leq 0.05$.

3. Results

There was no statistically significant difference in the number of parvalbumin-expressing interneurons of the suprapyramidal and infrapyramidal part of gyrus dentatus in the rats with PD cholinopathy (PPT lesion) or the hemiparkinsonian rats (SNpc lesion) versus the controls ($X^2 \geq 1.90$; $p \geq 0.29$; Fig. 3). However, in each experimental group the infrapyramidal part of gyrus dentatus had a smaller number of parvalbumin-expressing interneurons versus its suprapyramidal part ($z \geq -2.13$; $p \leq 0.03$; Fig. 3).

All the images of the gyrus dentatus granular layer of the hemiparkinsonian rats (SNpc lesion) exhibited increased dendritic arborization compared to the controls and the rats with PD cholinopathy (PPT lesion); their individual examples are depicted in Fig. 1, bottom panels.

We compared the fractal and GLCM features for each layer of the gyrus dentatus (suprapyramidal vs. infrapyramidal) within each experimental group (Table 1), and between the experimental groups (Control, PPT lesion, SNpc lesion; Table 2). All the statistically significant values are highlighted in bold.

Whereas the fractal parameters did not show consistent statistically significant differences between the groups ($z \geq -1.80$; $p \geq 0.07$), except for the Λ_{gray} value for the SNpc group, and the Λ_{bin} value for the PPT group of the suprapyramidal layer images ($z \geq -2.68$; $p \leq 0.01$), the binary fractal features differentiated the layers within the control group with significantly higher D_{out} and lower Λ_{bin} values ($z \geq -2.31$; $p \leq 0.05$) for the infrapyramidal layer, suggesting the greater morphological complexity of the contours in that layer.

In contrast to the fractal analysis, the GLCM features exhibited better performance. For the suprapyramidal layer of the gyrus dentatus *ASM* and *Entropy* differentiated the images of the SNpc lesion versus the images of the control and PPT lesion subjects with significantly higher *ASM* and lower *Entropy* ($z \geq -2.31$; $p \leq 0.03$), indicating the homogenization of images and their lower gray-level complexity. Although the *Contrast* was significantly higher and *IDM* was significantly lower for the suprapyramidal images of the PPT lesion group ($z \geq -1.97$; $p \leq 0.05$), none of the remaining texture parameters exhibited significant differences ($z \geq -1.64$; $p \geq 0.10$).

On the other hand, the infrapyramidal images of the SNpc group were differentiated compared to the images from the control and PPT groups for all GLCM parameters: they showed lower mean *Entropy* and *Contrast* ($z \geq -2.80$; $p \leq 0.03$) and higher *ASM*, *Correlation* and *IDM* ($z \geq -2.54$; $p \leq 0.04$). These results strongly suggest an increase in the uniformity, homogeneity and orderliness in the gray-levels of images from the SNpc group.

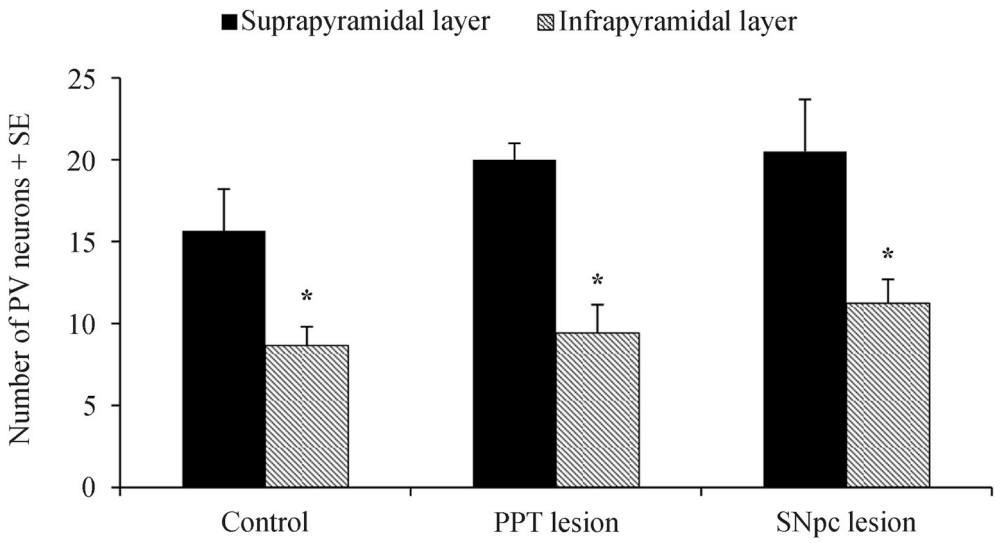

Fig. 3. Quantification of the parvalbumin-expressing GABA interneurons in the suprapyramidal and infrapyramidal part of the gyrus dentatus.
* indicates statistical significance at $p \leq 0.05$.

Table 1
The mean values of the fractal and gray level co-occurrence matrix (GLCM) parameters of the suprapyramidal and infrapyramidal layers of the hippocampal gyrus dentatus in: control rats (Control; n = 47 images from 5 rats), rats with Parkinson disease (PD) cholinergic neuropathology (PPT lesion; 35 images from 4 rats), and hemiparkinsonian rats (SNpc lesion; n = 41 images from 4 rats).

	D_{gray}	Λ_{gray} (x10^{-2})	D_{bin}	D_{out}	Λ_{bin} (x10^{-2})	*ASM* (x10^{-4})	Contrast	*Correlation* (x10^{-4})	IDM	Entropy
Control										
Suprapyramidal layer	1.37	5.65	1.70	1.49	69.27	9.04	35.71	12.01	0.27	7.57
Infrapyramidal layer	1.37	5.55	1.70	1.52	**61.62**	**7.51**	**40.41**	11.76	**0.24**	**7.74**
PPT lesion										
Suprapyramidal layer	1.37	5.63	1.71	1.51	61.56	8.04	37.66	11.75	0.24	7.66
Infrapyramidal layer	**1.36**	5.46	1.70	1.51	57.66	8.06	38.20	11.95	0.24	7.67
SNpc lesion										
Suprapyramidal layer	1.36	6.43	1.70	1.47	68.07	10.46	31.76	12.09	0.29	7.49
Infrapyramidal layer	1.36	5.79	1.72	1.50	**58.71**	9.43	34.52	12.26	**0.26**	7.54

Bold numbers indicate statistically significant differences between the suprapyramidal and infrapyramidal layers of the hippocampal gyrus dentatus within each experimental group at $p \leq 0.05$.

Table 2
The mean values of the fractal and gray level co-occurrence matrix (GLCM) parameters of the suprapyramidal and infrapyramidal layers of the hippocampal gyrus dentatus in: control rats (Control; n = 47 images from 5 rats), rats with Parkinson disease (PD) cholinergic neuropathology (PPT lesion; 35 images from 4 rats), and the hemiparkinsonian rats (SNpc lesion; n = 41 images from 4 rats).

	D_{gray}	Λ_{gray} (x10^{-2})	D_{bin}	D_{out}	Λ_{bin} (x10^{-2})	*ASM* (x10^{-4})	Contrast	*Correlation* (x10^{-4})	IDM	Entropy
suprapyramidal layer										
Control	1.37	5.65	1.70	1.49	69.27	9.04	35.71	12.01	0.27	7.57
PPT lesion	1.37	5.63	1.71	1.51	**61.56**	8.04	**37.66**	11.75	0.24	7.66
SNpc lesion	1.36	**6.43**	1.70	1.47	68.07	**10.46**	31.76	12.09	0.29	**7.49**
infrapyramidal layer										
Control	1.37	5.55	1.70	1.52	61.62	7.51	40.41	11.76	0.24	7.74
PPT lesion	1.36	5.46	1.70	1.51	57.66	8.06	38.20	11.95	0.24	7.67
SNpc lesion	1.36	5.79	1.72	1.50	58.71	**9.43**	**34.52**	**12.26**	**0.26**	**7.54**

Bold numbers indicate statistically significant differences between the suprapyramidal layers of the hippocampal gyrus dentatus in all experimental groups, and between the infrapyramidal layers of the hippocampal gyrus dentatus in all experimental groups at $p \leq 0.05$.

Moreover, these parameters, with the exception of *Correlation*, differentiated the layers within the control group. The infrapyramidal layer had lower *ASM*, and *IDM* ($z \geq -2.70$; $p \leq 0.01$) versus higher *Contrast* and *Entropy* ($z \geq -3.10$; $p \leq 0.004$), which is in agreement with their binary fractal parameters (D_{out}, Λ_{bin}), additionally suggesting the greater complexity of the gray-levels in the images of the infrapyramidal layer of the control gyrus dentatus. Such pronounced differences between layers were not observed within the images of the PPT and SNpc groups.

4. Discussion

Our present study shown that the GLCM and some fractal features are able to successfully differentiate the brain tissue textures of the suprapyramidal and infrapyramidal layers of the gyrus dentatus in the control rats, as well as in the rats with PD cholinopathy (PPT lesions) and hemiparkinsonian rats (with SNpc lesions).

In recent years, besides fractal analysis [12,23,24], GLCM analysis has found its application in terms of histological textures [3,4]. These analyses were selected based on their proven applicability to the

morphological classification of complex histological structures [25–27].

Although the fractal and GLCM analyses are classified as texture analysis tools, their implementation is evidently focused on different aspects of the image. Whereas fractal analysis deals with the complexity of contours and shapes, GLCM analysis accentuates the pixel position and intensity relationships, and the observed difference mainly comes from gray-level intensities and to a lesser extent from the morphological features of the sample.

The difference in the texture complexity of the suprapyramidal versus the infrapyramidal layer of the hippocampal gyrus dentatus images in all the experimental groups, and the change in that complexity caused by the experimentally induced neurodegenerative disease in the rats (either PD cholinopathy or hemiparkinsonism), is the major finding of this study.

Within the control group, the infrapyramidal layer images exhibited a more complex texture, as was shown by the GLCM parameters with their higher mean *Entropy* and *Contrast* values and their lower mean *ASM* and *IDM* values, as well as the higher mean value of the fractal D_{out} parameter. Whereas the higher values of *Entropy* indicate the presence of more information in the image texture, alongside the more spatially complex distribution of the gray-levels, the higher values of *Contrast* correspond to larger differences in the gray-levels, which may emerge as a result of the slightly more complex patterns of a given image. Regarding complexity, this is in accordance with the lower mean values of *ASM* and *IDM*, which correspond to both a uniformity of texture and its local homogeneity, respectively. The infrapyramidal layer also exhibited slightly more morphologically complex contours for those objects in the binary images with higher mean values of D_{out}, versus a lower mean value of $\Lambda_{bin,}$ which could be the result of the proliferation of gaps in a texture. This adds to the significant complexity difference in the layers within the control group, which was not observed to a similarly pronounced degree in the PPT (PD cholinopathy) and SNpc (hemiparkinsonism) groups, suggesting that this homogenization and loss of complexity in the infrapyramidal layer of the gyrus dentatus might have resulted from distant brain tissue damage (in this case, the distinctly experimentally induced neurodegenerative diseases).

In contrast to all the GLCM parameters that significantly differentiated the infrapyramidal layer images of the SNpc group versus the control and PPT groups, there were no changes in the fractal parameters.

Whereas the images of the suprapyramidal layer of the SNpc group exhibited lower mean values of *Entropy* vs. higher mean *ASM* values, the images of the infrapyramidal layer exhibited significantly lower mean values of *Entropy* and *Contrast* and higher mean values of *ASM*, *Correlation* and *IDM*, corresponding to a reduction in complexity and a rise in the orderliness, homogeneity and uniformity of the texture. Since we have demonstrated the smaller number of parvalbumin stained GABA interneurons in the infrapyramidal vs. the suprapyramidal layer of the hippocampal gyrus dentatus in all the experimental groups (Fig. 3), this result could in part emerge from the fact that the SNpc images showed pronounced dendritic arborizations (Fig. 2), as a consequence of the compensation for the loss of function at the lesion site, which affected the gray-levels of the texture by increasing the *IDM* and *ASM* values, thus making it more homogenous.

5. Conclusions

Our present results indicate that GLCM analysis is a more sensitive tool than fractal analysis for the detection of augmented dendritic arborization in histological images.

Declaration of competing interest

All the authors declare that they have no conflict of interest.

Acknowledgement

This work was supported by the Serbian Ministry of Education, Science and Technological Development Grant OI 173022.

References

[1] A. Kassner, R.E. Thornhill, Texture analysis: a review of neurologic MR imaging applications, Am. J. Neuroradiol. 31 (2010) 809–816, https://doi.org/10.3174/ajnr.A2061.
[2] M.S. de Oliveira, L.E. Betting, S.B. Mory, F. Cendes, G. Castellano, Texture analysis of magnetic resonance images of patients with juvenile myoclonic epilepsy, Epilepsy Behav. 27 (2013) 22–28, https://doi.org/10.1016/j.yebeh.2012.12.009.
[3] I. Pantic, S. Dacic, P. Brkic, I. Lavrnja, T. Jovanovic, S. Pantic, S. Pekovic, Discriminatory ability of fractal and grey level co-occurrence matrix methods in structural analysis of hippocampus layers, J. Theor. Biol. 370 (2015) 151–156, https://doi.org/10.1016/j.jtbi.2015.01.035.
[4] I. Pantic, S. Dacic, P. Brkic, I. Lavrnja, S. Pantic, T. Jovanovic, S. Pekovic, Application of fractal and grey level Co-occurrence matrix analysis in evaluation of brain corpus callosum and cingulum architecture, Microsc. Microanal. 20 (2014) 1373–1381, https://doi.org/10.1017/S1431927614012811.
[5] B.B. Mandelbrot, The Fractal Geometry of Nature, 1983, https://doi.org/10.1017/CBO9781107415324.004.
[6] A. Di Ieva, The Fractal Geometry of the Brain, Springer, 2016, p. 585, https://doi.org/10.1007/978-1-4939-3995-4.
[7] A. Badea, A.A. Ali-Sharief, G.A. Johnson, Morphometric analysis of the C57BL/6J mouse brain, Neuroimage 37 (2007) 683–693, https://doi.org/10.1016/j.neuroimage.2007.05.046.
[8] N. Sarkar, B.B. Chaudhuri, An efficient differential box-counting approach to compute fractal dimension of image, IEEE Trans. Syst. Man. Cybern. 24 (1994) 115–120, https://doi.org/10.1109/21.259692.
[9] M.H. Bharati, J.J. Liu, J.F. MacGregor, Image texture analysis: methods and comparisons, Chemometr. Intell. Lab. Syst. 72 (2004) 57–71, https://doi.org/10.1016/j.chemolab.2004.02.005.
[10] B. Julesz, Experiments in the visual perception of texture, Sci. Am. 232 (1975) 34–43. http://www.jstor.org/stable/24949771.
[11] R.M. Haralick, K. Shanmugam, I. Dinstein, Textural features for image classification, IEEE Trans. Syst. Man. Cybern. SMC-3 (1973) 610–621, https://doi.org/10.1109/TSMC.1973.4309314.
[12] N. Rajković, D. Kolarević, K. Kanjer, N.T. Milošević, D. Nikolić-Vukosavljević, M. Radulovic, Comparison of Monofractal, Multifractal and gray level Co-occurrence matrix algorithms in analysis of Breast tumor microscopic images for prognosis of distant metastasis risk, Biomed. Microdevices 18 (2016), https://doi.org/10.1007/s10544-016-0103-x.
[13] G. Paxinos, C. Watson, The Rat Brain in Stereotaxic Coordinates, fifth ed., Elsevier Academic Press, San Diego, CA, 2005.
[14] J. Ciric, K. Lazic, S. Kapor, M. Perovic, J. Petrovic, V. Pesic, S. Kanazir, J. Saponjic, Sleep disorder and altered locomotor activity as biomarkers of the Parkinson's disease cholinopathy in rat, Behav. Brain Res. 339 (2018) 79–92, https://doi.org/10.1016/j.bbr.2017.11.021.
[15] J. Ciric, S. Kapor, M. Perovic, J. Saponjic, Alterations of sleep and sleep oscillations in the hemiparkinsonian rat, Front. Neurosci. 13 (2019) 148, https://doi.org/10.3389/fnins.2019.00148.
[16] J. Ciric, K. Lazic, J. Petrovic, A. Kalauzi, J. Saponjic, Sleep spindles as an early biomarker of REM sleep disorder in a rat model of Parkinson's disease cholinopathy, Transl. Brain Rhythm. 2 (2017) 1–11, https://doi.org/10.15761/TBR.1000111.
[17] G. Paxinos, C. Watson, P. Carrive, M.T.K. Kirkcaldie, K. Ashwell, Chemoarchitectonic Atlas of the Rat Brain, second ed., Academic Press, London, UK, 2009.
[18] J.E. Cabrera, Texture analyzer image J plugin. https://imagej.nih.gov/ij/plugins/texture.html, 2006 (Accessed 04-18-2018).
[19] M. Hall-Beyer, GLCM Texture: A Tutorial v. 3.0 March 2017 [Internet], University of Calgary, 2017. Available from: http://rgdoi.net/10.13140/RG.2.2.12424.21767.
[20] A.L. Karperien, FracLac for ImageJ. http://rsb.info.nih.gov/ij/plugins/fraclac/FLHelp/Introduction.htm, 2013.
[21] T.G. Smith, G.D. Lange, W.B. Marks, Fractal methods and results in cellular morphology - dimensions, lacunarity and multifractals, J. Neurosci. Methods 69 (1996) 123–136, https://doi.org/10.1016/S0165-0270(96)00080-5.
[22] E.R. Weibel, Fractal geometry: a design principle for living organisms, Am. J. Physiol. 261 (1991) L361–L369. http://www.ncbi.nlm.nih.gov/pubmed/1767856.
[23] N. Rajković, X. Li, K.N. Plataniotis, K. Kanjer, M. Radulovic, N.T. Milošević, The pan-cytokeratin staining intensity and fractal computational analysis of breast tumor malignant growth patterns prognosticate the occurrence of distant metastasis, Front. Oncol. 8 (2018) 348, https://doi.org/10.3389/fonc.2018.00348.
[24] A.N. Esgiar, R.N.G. Naguib, B.S. Sharif, M.K. Bennett, A. Murray, Fractal analysis in the detection of colonic cancer images, IEEE Trans. Inf. Technol. Biomed. 6 (2002) 54–58, https://doi.org/10.1109/4233.992163.
[25] I. Pantic, D. Nesic, D. Stevanovic, V. Starcevic, S. Pantic, V. Trajkovic, Effects of ghrelin on the structural complexity of exocrine pancreas tissue architecture,

Microsc. Microanal. 19 (2013) 553–558, https://doi.org/10.1017/S1431927613000524.

[26] I. Pantic, J. Paunovic, G. Basta-Jovanovic, M. Perovic, S. Pantic, N.T. Milosevic, Age-related reduction of structural complexity in spleen hematopoietic tissue architecture in mice, Exp. Gerontol. 48 (2013) 926–932, https://doi.org/10.1016/j.exger.2013.06.011.

[27] M. Tambasco, B.M. Costello, A. Kouznetsov, A. Yau, A.M. Magliocco, Quantifying the architectural complexity of microscopic images of histology specimens, Micron 40 (2009) 486–494, https://doi.org/10.1016/j.micron.2008.12.004.